X-723-75-249
PREPRINT

WAVEGUIDE CO_2 LASER GAIN: DEPENDENCE ON GAS KINETIC AND DISCHARGE PROPERTIES

STEVEN C. COHEN

SEPTEMBER 1975

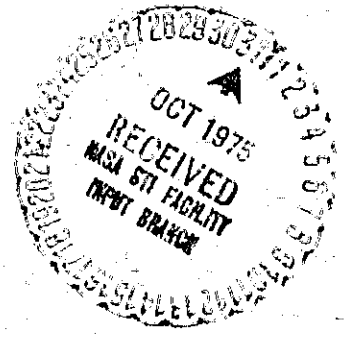

GSFC
GODDARD SPACE FLIGHT CENTER
GREENBELT, MARYLAND

WAVEGUIDE CO_2 LASER GAIN:

DEPENDENCE ON GAS KINETIC AND DISCHARGE PROPERTIES

Steven C. Cohen

Laser Technology Branch

Goddard Space Flight Center

Greenbelt, Maryland 20771

ABSTRACT

Using a simple rate equation approach we examine the gas kinetic and discharge properties of waveguide CO_2 lasers. We calculate the dependence of the population inversion and laser small signal gain on gas pressure, gas mixture, pumping rate (discharge current), tube bore diameter, and wall temperature. The results indicate, for example, that at a pressure of 50 torr the gain is maximized with a gas mixture in the ratio $CO_2:N_2:He \sim 0.75:1:1.5$, a tube bore diameter of ~ 0.07 cm and a discharge current density of ~ 500 ma/cm^2. At higher pressures the gain is optimized by using more helium rich mixtures and smaller bore diameters. We also calculate the dependence of laser tunability on the gas kinetic properties and cavity losses. We find that for low loss cavities the laser tunability may substantially exceed the molecular fullwidth at half maximum. Furthermore, the more helium rich gas mixtures give greater tunability when cavity losses are small and less tunability when cavity losses

are large. The role of the various gases in the waveguide CO_2 laser is the same as that in conventional devices. By contrast with conventional lasers, however, the waveguide laser transition is homogeneously broadened. Thus the dependence of gain on gas pressure and other kinetic and discharge properties differs substantially from that predicted by scaling results from conventional low pressure lasers.

WAVEGUIDE CO_2 LASER GAIN: DEPENDENCE ON GAS KINETIC AND DISCHARGE PROPERTIES

I. INTRODUCTION

The waveguide CO_2 laser is a compact, high gain, tunable CO_2 laser. It is an attractive device for many applications including, in particular, laser communications and high resolution spectroscopy. For these applications it is essential to know the variations in laser gain and tunability with gas mixture, pressure discharge current, bore diameter, and wall temperature.

We will calculate the gain in CO_2-N_2-He waveguide lasers using an approach which centers around the rate equations for the vibrational modes of the CO_2 and N_2 molecules. Our analysis draws heavily on the formulation of Gordietz et al.[1] and Moore et al.[2] for conventional lasers. The essential differences here are the smaller tube bore diameters, higher gas pressures, and higher current densities. These differences manifest themselves in faster rates of electron-molecule and molecule-molecule energy transfer and in a faster diffusion rate to the tube wall. The higher operating pressures also insure that the gas is homogeneously broadened in contrast to the inhomogeneous broadening of low pressure (several torr) devices.

Before proceeding with this paper we should point out that the gas discharge scaling laws[3-4] can also provide much information about waveguide lasers via

a transformation to a laser with a larger tube diameter whose characteristics have been completely determined. Thus for example, a laser with a 0.1 cm bore diameter, current density of 150 ma/cm^2 and with a total gas pressure of 100 torr is similar to one with a 1 cm bore, 15 ma/cm^2 current density, gas pressure of 10 torr, and with the same gas mixture. While the two discharges have the same relative population level distributions, their gains differ due to the different absolute population levels and different broadening mechanisms. Furthermore, the scaling laws may be difficult to apply for practical computation of gain since complete characterization of all the required similar discharges is rarely available.

In the next section of this paper we discuss the theory of laser kinetics, then in Section III we will discuss the numerical techniques employed in gain computations. In Section IV we present and analyze selected computational results which illustrate the dependence of laser gain on the external parameters. Section V contains our concluding remarks.

II. THEORY

The relevant features of the familiar CO_2-N_2 vibrational energy level diagram are shown in Figure 1. We assume that both the vibrational mode of N_2 and the asymmetric stretch mode (ν_3) of CO_2 are excited by electron impact. Energy exchange between the excited N_2 molecules and the ν_3 mode of CO_2 occurs via nearly resonant V-V energy transfer. Rapid intramode relaxation assures that

the energy level occupancy of the ν_3 mode is characterized by a Boltzmann distribution at temperature T_3. The fraction, $f_2(T_3)$, of the CO_2 molecules whose asymmetric stretch mode is excited are in the upper lasing level (designated 001). Deexcitation of the ν_3 mode occurs both via molecular collisions and wall interactions. The molecular collisions result in the excitation of the ν_1 and ν_2 modes which are assumed to maintain equilibrium due to the rapid Fermi resonance interaction. The equilibrium distribution is characterized by the temperature T_2. A fraction, f_1, of the molecules in the combined ν_{12} mode is in the lower laser level (assumed in the present calculation to be the 100 level). Deexcitation of the ν_{12} mode occurs via diffusion loss to the walls and via molecular energy transfer, in particular via V-T processes from the 010 level. Thus for a fixed gas mixture, total pressure, and electron temperature, the system is described by the density, n_2, of CO_2 molecules in the ν_3 mode, the density, n_1, of CO_2 molecules in the ν_{12} mode, the density of excited nitrogen molecules, N_2^*, kinetic temperature. The vibrational population inversion is $\Delta n = f_2\, n_2 - f_1\, n_1$

With symbols defined in Table I the steady state rate equations are

$$\frac{dn_2}{dt} = \alpha n_0 - \rho n_2 + K n_0 N_2^* - K n_2 N_2^0 + K_{12} n_1 - K_{21} n_2 - \frac{\beta_2 D_{CO_2}}{\Lambda^2} n_2 = 0 \qquad \text{(1a)}$$

$$\frac{dn_1}{dt} = \omega K_{21} n_2 - \omega K_{12} n_1 + \tfrac{1}{2} K_{01} n_0 - \tfrac{1}{2} K_{10} n_0 - \frac{\beta_1 D_{CO_2}}{\Lambda^2} n_1 = 0 \qquad \text{(1b)}$$

$$\frac{dN_2^*}{dt} = \gamma N_2^0 - \zeta N_2^* - Kn_0 N_2^* + Kn_2 N_2^0 - \frac{\beta_{N_2} D_{N_2}}{\Lambda^2} N_2^* = 0 \qquad (1c)$$

The first two terms in Equation (1a) are the electron excitation and deexcitation of the CO_2 ν_3 mode. The next two terms give the resonant exchange between ν_3 and the excited N_2 molecules, the terms with K_{21} and K_{12} express the energy transfer between the ν_3 and ν_{12} modes, and the final term represents the deexcitation due to diffusion to the walls. In Equation (1b) the terms containing K_{10} and K_{01} express the relaxation and excitation of the ν_{12} mode to and from the ground state, and the final term is the diffusion loss. Finally in Equation (1c) the first two terms give the rate of vibrational excitation and deexcitation of nitrogen due to electron impact, and the last term is again a diffusion loss. In the present work we do not consider the decomposition of CO_2 in the laser discharge.

Several of the numerical coefficients appearing in Equations (1a-1c) require more detailed explanation. Each of the diffusion terms contains a numerical coefficient, β, which is an estimate of the average number of quanta lost per wall deexcitation of that mode. Thus, for example, Gordietz et al.[1] have estimated that, on the average, 1.5 quanta of ν_3 oscillation are lost in a wall deexcitation of n_2, i.e., $\beta_2 = 1.5$. The coefficient ω appearing in front of the $K_{21} n_2$ and $K_{12} n_1$ terms in Equation (1b) takes into account the fact that a molecular collision deactivation of the ν_3 mode in favor of the ν_{12} mode usually results

in the excitation of more than 1 quanta of ν_{12} oscillation (We consider 2 quanta of ν_2 oscillation to be equivalent to 1 quanta of ν_1 oscillation.). Typical deexciting reactions include

$$(001) + M \rightarrow (030) + M \tag{2a}$$

$$(001) + M \rightarrow (040) + M \tag{2b}$$

$$(001) + M \rightarrow (110) + M \tag{2c}$$

where M can be a CO_2, N_2, or He molecule. Reactions (2a) and (2c), for example, result in a factor 3/2 appearing before the $K_{21} n_2$ and $K_{12} n_1$ terms in Equation (1b); reaction (2b) results in a factor of 2. The factor 1/2 appearing in the third and fourth terms of Equation (1c) can be explained by considering the collisional deactivation of the ν_{12} mode which occurs primarily through the reaction

$$(010) + M \rightarrow (000) + M \tag{3}$$

where, in most cases, helium is the dominant collision partner. Since each deactivation of one ν_2 quanta via the reaction described by Equation (3) is equivalent to the deactivation of only 1/2 quanta of ν_1 oscillation, and since the (100) state is the lower laser state, terms $K_{10} n_1$ and $K_{01} n_0$ have to be multiplied by a factor of 1/2.

A few comments should be made about the collision rate constants K_{21} and K_{10} which refer to the relaxation rate of the ν_3 mode to the ν_{12} mode and the

ν_{12} mode to ground respectively. Each rate is a composite sum of reaction rates with each of the gas constituents, e.g.,

$$K_{21} = K_{21}^{CO_2} P_{CO_2} + K_{21}^{N_2} P_{N_2} + K_{21}^{He} P_{He} \tag{4}$$

where the specific rate constants, K_{21}^{X}, are given in units of (torr-sec)$^{-1}$ and the P_X's are the partial pressures of the gases. Each of these specific rate constants can be, in turn, the sum of several reactions. For example, three prime contributors to K_{21} are given by reactions (2a-2c).

With the exception of the inclusion of diffusion terms in the rate equations we have, to this point, ignored any spatial variation of the electron and molecule densities. We will now assume that the discharge electrons and the excited states of CO_2 and N_2 have a zero order Bessel function radial distribution, $J_0\left(\frac{r}{\Lambda}\right)$, which is centered on the bore axis. Then redefining n_1, n_2, and N_2^* so they refer to the on axis (peak) density, the rate equations become

$$an_0[1] - \rho n_2[2] + Kn_0 N_2^*[1] - Kn_2 N_2^0[1] - K_{12} n_1[1] + K_{21} n_2[1] - \beta_2 \frac{D_{CO_2}}{\Lambda^2} n_2[1] = 0 \tag{5a}$$

$$\omega K_{21} n_2[1] - \omega K_{12} n_1[1] + \tfrac{1}{2} K_{01} n_0 - \tfrac{1}{2} K_{10} n_2[1] - \beta_1 \frac{D_{CO_2}}{\Lambda^2} n_1[1] = 0 \tag{5b}$$

$$\gamma N_2^0[1] - \zeta N_2^*[2] - Kn_0 N_2^*[1] + Kn_2 N_2^0[1] - \beta_{N_2} \frac{D_{N_2}}{\Lambda^2} N_2^*[1] = 0 \tag{5c}$$

where

$$[1] = \frac{1}{\pi R^2} \int_0^{2\pi} d\phi \int_0^R r J_0\left(\frac{r}{\Lambda}\right) dr \approx 0.434$$

$$[2] = \frac{1}{\pi R^2} \int_0^{2\pi} d\phi \int_0^R r J_0^2\left(\frac{r}{\Lambda}\right) dr \approx 0.270$$

and where a, ρ, γ, and ζ, which are proportional to electron density, now also refer to the on-axis (peak) excitation and deexcitation rates. Equations (5a-5c) can be cast in the form of Equation (1a-1c) by dividing each equation by [1] and defining

$$\rho' = \rho[2]/[1] \tag{6a}$$

$$K''_{01} = K_{01}/[1] \tag{6b}$$

$$\zeta' = \zeta[2]/[1] \tag{6c}$$

We then reproduce Equations (1a-1c) with ρ', K''_{01}, ζ' replacing ρ, K_{01}, ζ. To this set of equations we add the equations for particle conservation, namely:

$$n = n_0 + n_1[1] + n_2[1] \tag{7a}$$

$$N_2 = N_2^0 + N_2^*[1] \tag{7b}$$

Now eliminating n_0 and N_2^0 by way of Equations (7), combining Equation (5a) and (5c) to eliminate N_2^*, and using Equation (5b) to express n_2 in terms of n_1 we

derive a quadratic expression for n_1:

$$n_1^2 [K''(a'' + \bar{s}\,\Omega)] - n_1 [K''(\gamma N_2 + an - \delta\Omega) + K\bar{s}\,\theta N_2 + (a'' + \bar{s}\,\Omega)(\theta + Kn)] - (\gamma N_2 + an - \delta\Omega)(\theta + Kn) - \theta N_2 (\gamma + K\delta) = 0 \quad (8)$$

where

$$\gamma'' = \gamma/[1] \quad (6d)$$

$$K'' = K/[1] \quad (6e)$$

$$a'' = a/[1] \quad (6f)$$

$$\bar{s} = \frac{\frac{K_{01}}{2} + \frac{K_{10}}{2} + \frac{\beta_1 D_{CO_2}}{\Lambda^2}}{\omega K_{21} - \frac{K_{01}}{2}} \quad (9)$$

$$\delta = \frac{-\frac{1}{2}K''_{01} n}{\omega K_{21} - \frac{K_{01}}{2}} \quad (10)$$

and

$$\Omega = a'' + \rho' + K_{21} + \beta_2 \frac{D_{CO_2}}{\Lambda^2} \quad (11)$$

$$\theta = \gamma'' + \zeta' + \beta_{N_2} \frac{D_{N_2}}{\Lambda^2} \quad (12)$$

In Equation (8) we have ignored the small excitation of the ν_3 mode from the ν_{12} mode.

The rate constants appearing in the preceeding equations are functions of the gas temperature. This temperature is controlled by the rate of energy transfer from electron to gas kinetic energy and by the gas thermal conductivity. We will ignore any spatial variation in the gas temperature and assume that all the energy transferred by electrons to molecular vibration contributes to the temperature rise after vibrational relaxation. We can write[1]

$$\Delta T = T - T_w = \frac{1.36R^2[\gamma N_2^* \cdot \zeta' N_2^* + an_2 - \zeta' n_0]}{18.9\kappa} E_3 \qquad (13)$$

where T_w is the wall temperature, E_3 is the energy of the ν_3 quantum, and κ is the thermal conductivity given by[1]

$$\kappa = \kappa_{CO_2}\left[1 + 0.81\frac{P_{N_2}}{P_{He}} + 0.23\frac{P_{He}}{P_{CO_2}}\right]^{-1} + \kappa_{N_2}\left[1 + 1.4\frac{P_{CO_2}}{P_{N_2}} + 0.34\frac{P_{He}}{P_{N_2}}\right]^{-1}$$
$$+ \kappa_{He}\left[1 + 3.4\frac{P_{CO_2}}{P_{He}} + 2.7\frac{P_{N_2}}{P_{He}}\right]^{-1} \qquad (14)$$

Equation (13) is an extension of the result quoted in reference 1; the extension takes into account the direct excitation of the ν_3 mode of the CO_2. The numerator of the equation is proportional to the heat input to the gas.

We have noted that the vibrational energy level population inversion is $(f_2n_2 - f_1n_1)$[1]. As of yet, however, we have not considered the rotational sublevels of

each vibrational level (except to implicitly assume that the rotational relaxation is very rapid compared to that of vibration). We now take explicit note of the Boltzmann distribution of rotational sublevels at the gas kinetic temperature, T. The vibration-rotation population inversion is

$$\Delta n_J = f_2 n_2 [\,] \frac{2hc\beta_2}{k_B T} d_2 e^{-J_2(J_2+1)\frac{hc\beta_2}{k_B T}} - f_1 n_1 [\,] \frac{2hc\beta_1}{k_B T} d_1 e^{-J_1(J_1+1)\frac{hc\beta_1}{k_B T}} \qquad (15)$$

where d_2 and d_1 are the degeneracies of the upper and lower state rotational sublevels, B_2 and B_1 and the sublevel energies (in cm^{-1}), J_2 and J_1 are the sublevel rotational quantum numbers, h is Planck's constant, c is the speed of light, and k_B is Boltzmann's constant.

Given the population inversion it is a simple matter to calculate the small signal gain, which for a homogeneously broadened laser line is

(16)

$$g(\nu) = \frac{\lambda^2 d_2}{8\pi t_s} \left\{ f_2 n_2 [\,] \frac{2hc\beta_2}{k_B T} e^{-J_2(J_2+1)\frac{hc\beta_2}{k_B T}} - f_1 n_1 [\,] \frac{2hc\beta_1}{k_B T} e^{-J_1(J_1+1)\frac{hc\beta_1}{k_B T}} \right\} \frac{\Delta\nu/2\pi}{(\nu-\nu_0)^2 + \left(\frac{\Delta\nu}{2}\right)^2}$$

where λ is the wavelength of the transition, t_s is the spontaneous emission lifetime, and $\Delta\nu$ is the linewidth. The gain is a function of the vibration-rotation inversion and the linewidth, both of which vary with temperature, gas mixture, and pressure. The inversion also depends on the discharge current (excitation rate) and the tube wall temperature.

Once we know the line center gain of a laser oscillator as well as the length of the gain medium and the reflectivity of the cavity mirrors, r_1 and r_2, then we can also determine the laser frequency tuning range from line center, Δf[5]

$$\Delta f = \frac{\Delta\nu}{2}\sqrt{\frac{g_0(\nu_0)L}{\ell n\left(\frac{1}{\sqrt{r_1 r_2}}\right)} - 1} \qquad (17)$$

III. COMPUTATIONAL AND NUMERICAL CONSIDERATIONS

While the theory developed in Section II is sufficiently detailed to accurately predict the dependence of laser gain, population inversion, and gas temperature on the kinetic and discharge properties of the laser, it also has simple computational requirements. In practice for a given gas mixture, total pressure, pump rate, and wall temperature, an initial estimate is made for the gas temperature (for simplicity our usual estimate is $T = T_w$). The quadratic equation for n_1 is solved, from which the other molecular state populations are computed. From this information we calculate an updated gas temperature using Equation (13). The updated temperature is then reinserted in the loop and iterative process continued until temperature convergence has been achieved. After convergence, we calculate f_2, f_1, $\Delta\nu$ and other parameters required to compute the gain. A flow diagram for this process appears in Figure 2.

This computational procedure has been programmed on an HP model 9820A desk top calculator with 429 storage register memory (About 3/4 of these

registers are required in the current version of our program.). Computation of the gain for a particular set of operating conditions requires, typically, a few seconds. The output is either plotted on an HP model 9862A plotter or written on paper tape. The program is input either by magnetic card or magnetic ta using the HP9865A cassette reader.

The rate constants which enter into our calculations are K, K_{21} (M = CO_2, N_2, He), K_{10} (M = CO_2, N_1, He), a, and γ. The rate constants for the inverse processes are determined by detailed balancing. The numerical values for the rate constants and other factors which we have used in our calculations can be found in the reference cited in Table II. * We have found, however, that the qualitative features of population inversion, gain, and gas temperature are insensitive to the exact values of the rate constants. Thus, for example, replacing the theoretical rate constants of reference 1 by the somewhat different experimental rate constants quoted in reference 11 produces little change in the qualitative dependence of gain on the independent variables.

We should note that in calculating the absolute magnitude of the gain the spontaneous emission lifetime for a particular P or R branch transition must be used. This quantity, t_s, is related to the radiative lifetime of the upper vibration-rotation level, t_2, by $\frac{1}{t_s} = \frac{S_J}{d_2}\frac{1}{t_2}$ where $S_J = J_2 + 1$ for a P branch transition and $S_J = J_2$ for an R branch transition.

*In addition we have chosen $\omega = 1.5$, $\beta_1 = 1.5$, $\beta_2 = 1.0$, $\beta_{N_2} = 1.5$.

IV. RESULTS

The gas population inversion, gain, gas temperature, and laser tunability have been computed as a function of gas mixture, total pressure, pump rate, bore diameter, and wall temperature. Space limitations require that we present here only selected results which illustrate the salient features of waveguide laser performance.

In Figure 3 we present the pressure dependence of gain for several gas mixtures. The small signal gain is evaluated for the line center of the P(20) 001 → 100 transition. We see that:

1. For each mixture there is an optimal operating pressure for maximum gain. The more helium rich the mixture, the higher the optimal pressure;
2. The maximum available gain tends to decrease with increasing helium fraction;
3. The more helium rich mixtures show less gain variations with pressure.

In Figure 3 we also reproduce for comparison purposes experimental data on the laser gain.[12] It is evident that the experimental and theoretical curves agree quite well.

In Figure 4, we plot the laser gain versus mixture for two total pressures. At fifty torr, the theoretical optimum gas mixture is very close to that found experimentally by Burkhardt, et al.[13] to be optimum, namely CO_2:N_2:He-1:06:1.4.

At 150 torr we find that a mixture in the approximate ratio 1:1:5-1:1:7 gives optimum gain even though less helium rich mixtures have higher gains at lower pressures. Since high laser tunability implies high operating pressures it is clear that the tunable CO_2 waveguides lasers require mixtures that give less than optimal gain at lower pressures. Figure 5 shows the dependence of gas temperature on fill pressure for three of the gas mixtures whose gain is plotted in Figure 3. It is apparent that the decreased sensitivity of the gain of helium rich mixtures to pressure increases is a reflection of cooler, less pressure dependent gas temperature. Furthermore, Figure 6 shows that the reason that these more helium rich mixtures are required at higher operating pressures is to prevent adversely large rises in the temperature. At 150 torr, the presence of helium in the laser discharge prevents a gas temperature rise of several hundred degrees above the wall temperature. At 50 torr, the potential temperature rise is less dramatic; as a consequence less helium is required in the gain optimized mixture. The role of helium in gas temperature control is, as in conventional CO_2 lasers, to enhance the gas thermal conductivity over that of an N_2 - CO_2 mixture.

Calculations of gain versus pump rate (discharge current) have revealed a somewhat decreasing gain sensitivity to pump rate variations at higher pressures. As shown in Figure 7 the gain for a 1:1:1.5 mixture at 50 torr and with a bore radius of 0.0625 cm rises to a peak at a nitrogen pump rate of about 14,000 sec^{-1}.

Assuming (very approximately) that the pump rate is related to the current density by $J = 0.016\gamma$ where J is in ma/cm^2 and γ is in sec^{-1}, we find this optimal pump rate corresponds to a current of about 2.7 ma. At 150 torr with a 1:1:5 mixture, the optimal pump rate is reduced to about 10,000 $sec.^{-1}$ corresponding to a current of about 2.0 ma.

Another factor influencing gain is the tube diameter. The decreased bore width of a waveguide as compared to a more conventional laser manifests itself in several competing effects. First since the walls are closer there is a greater rate of molecular diffusion to the walls with subsequent vibrational deexcitation; second, the thermal transport of energy out of the discharge is more rapid; and finally there is a higher current density. Figure 8 shows the variation in laser gain as the bore diameter is changed but with the pressure and current held fixed. It is evident that for each pressure there is an optimal bore diameter and current which maximizes the gain. In general, however, smaller bore diameters permit operation at higher gas pressures.

As expected and shown in Figure 9 the laser wall temperature has significant impact on gain. With lower wall temperatures, the excited gas remains cooler; hence there are fewer adverse vibrational deexcitations and the population inversion and gain are greater. We find for example, that for a 1:1:1.5 mixture at 50 torr that the gain increases from 1.7%/cm, to 2.9%/cm as the wall temperature is lowered from 350 K to 250 K.

In Figure 10 we plot the laser tunability as a function of pressure. The parameter $\frac{2}{L} \ell n \left[\frac{1}{\sqrt{r_1 r_2}}\right]$ is approximately equal to the loss divided by cavity length. It is important to note that for high losses the less helium rich mixtures provide maximum tunability while for low losses the non helium rich mixtures are preferred. Thus for example, with a loss of 0.2%/cm the 1:0.5:3 mixture has a maximum tunability of 460 MHz at 110 torr while the 1:0.5:6 mixture has a maximum tunability of 300 MHz at 125 torr. By contrast, with a loss of 0.5%/cm the 1:0.5:3 mixture has a maximum tunability of 1600 MHz at 160 torr while the 1:0.5:6 mixture has a tunability of 1780 MHz at 240 torr. In all cases it is apparent that the tunability peaks at some optimal pressure, a consequences of the dependence of both the gain and the linewidth on pressure. The value of the optimal pressure and the associated tunability depends on the cavity losses and length.[5]

V. CONCLUDING REMARKS

The role of the three gases in the waveguide laser mixture is essentially the same as in conventional lasers. The nitrogen acts as a pump for the inversion in CO_2. The helium assures rapid depopulation of the lower laser level and increases the gas thermal conductivity over that of CO_2 - N_2 mixtures.

The population inversion in the laser discharge is determined by the competition among several kinetic processes including electron-molecule collisions, inter- and intramolecule energy transfer, molecular diffusion, and molecule-wall

interaction. In particular the diffusion to the walls and subsequent deexcitation as well as direct collisional deexcitation are responsible for the vibrational deactivation of the CO_2 molecule. At low pressures the diffusion loss dominates the deexcitation. As the pressure increases the rate of collisional deexcitation increases, but the diffusion rate is reduced; hence wall losses become less significant and collisional deexcitation dominates. At the higher operating pressures collisions further reduce the gain by homogeneous broadening of the laser transition. Thus the gain peaks at substantially lower pressures than does the population inversion.

The author wishes to express his appreciation to John Degnan and Walter Leeb for stimulating discussions on several aspects of the work.

REFERENCES

1. a. B. F. Gordietz, N. N. Sobolev, V. V. Sokovikov, and L. A. Shelepin, Phys. Letters, 25A, 173 (1967)

   b. B. F. Gordietz, N. N. Sobolev, and L. A. Shelepin, Sov. Phys. JETP, 26, 1039 (1968)

   c. B. F. Gordietz, N. N. Sovolev, V. V. Sokovikov, and L. A. Shelepin, IEEE J. Quantum Electronics, QE-4, 796 (1968)

   d. See also J. Tulip, IEEE J. Quantum Electronics, QE-6, 206 (1970)

2. C. B. Moore, R. E. Wood, B. L. Hu, and Y. T. Yardley, J. Chem. Phys., 46, 4222 (1967)

3. V. K. Konyukhov, Sov. Phys. - Tech. Phys., 15, 1283 (1971)

4. R. L. Abrams and W. B. Bridges, IEEE J. Quantum Electronics, QE-9, 940, (1973)

5. J. J. Degnan, J. App. Phys., 45, 757 (1974)

6. W. A. Rosser, A. D. Wood, and E. T. Gerry, J. Chem. Phys., 50, 4996 (1969)

7. American Institute of Physics Handbook 3rd Ed., McGraw Hill (1972)

8. O. Judd, Hughes Research Laboratories Internal Research Report No. 452 (1971)

9. R. A. McClatchey, W. S. Benedict, S. A. Clough, D. E. Burch, R. F. Calfee, K. Fox, L. S. Rothman, and J. S. Garing, AFCRL Technical Report 73-0096 (1973)

10. C. P. Christensen, C. Freed, H. A. Haus, IEEE J. Quantum Electronics, QE-5, 276 (1969) and references therein

11. R. L. Taylor and S. Bitterman, Rev. Mod. Phys., 41, 26 (1969)

12. Hughes Aircraft Company, Design Report for NASA Contract NAS 5-20623 (1975)

13. E. G. Burkhardt, T. J. Bridges, and P. W. Smith, Optics Communications, 6, 193 (1972)

Figure Captions

Figure 1. Energy level diagram for low lying vibrational states of CO_2 and N_2. The combined population density of the CO_2 bending and symmetric stretching modes (assumed in equilibrium) is n_1; the population densities of the CO_2 asymmetric mode, CO_2 ground state, N_2 excited states, and N_2 ground state are n_2, n_0, N_2^*, and N_2^0 respectively.

Figure 2. Logic flow diagram for computation of laser kinetic and discharge properties

Figure 3. Small signal gain versus fill pressure for several gas mixtures. Gain is evaluated at line center assuming homogeneous line broadening. The experimental points are extracted from reference 12. We assume that $\gamma = 10,000\ sec^{-1}$ corresponds to a current of 2-3 ma for a 0.0625 cm bore radius.

Figure 4. Small signal gain versus mixture for total fill pressure of (a) 50 torr (b) 150 torr

Figure 5. Temperature versus fill pressure for several gas mixtures

Figure 6. Temperature versus gas mixture of fill pressures of 50 and 150 torr

Figure 7. Small signal gain versus pump rate

Figure 8. Small signal gain versus tube bore diameter.
1. pressure = 50 torr, $\gamma R^2 = 39$
2. pressure = 100 torr, $\gamma R^2 = 39$
3. pressure = 150 torr, $\gamma R^2 = 39$
4. pressure = 50 torr, $\gamma R^2 = 117$
5. pressure = 100 torr, $\gamma R^2 = 117$
6. pressure = 150 torr, $\gamma R^2 = 117$

$\gamma R^2 = 39$ (117) corresponds approximately to a current of 2 (6) ma.

Figure 9. Small signal gain versus wall temperature

Figure 10. Laser tunability, $2\Delta f_1$, versus fill pressure. The parameter $\frac{2}{L}\ell n\sqrt{r_1 r_2}$ is essentially the loss per unit length divided by cavity length

(a) gas mixture $CO_2:N_2:He$ - 1:0.5:3

(b) gas mixture $CO_2:N_2:He$ - 1:0.5:6

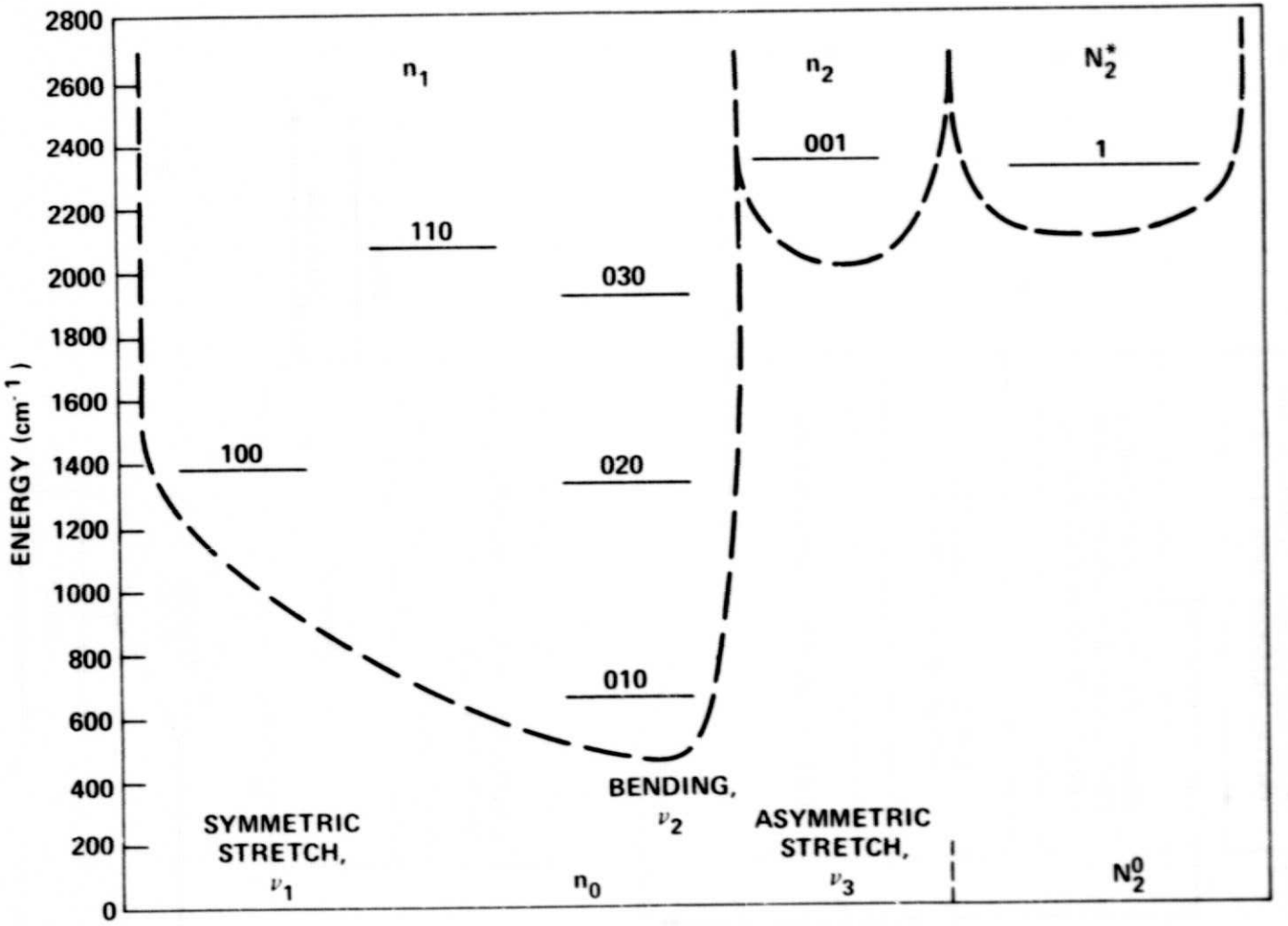

Figure 1. Energy level diagram for low lying vibrational states of CO_2 and N_2. The combined population density of the CO_2 bending and symmetric stretching modes (assumed in equilibrium) is n_1; the population densities of the CO_2 asymmetric mode, CO_2 ground state, N_2 excited states, and N_2 ground state are n_2, n_0, N_2^*, and N_2^0 respectively.

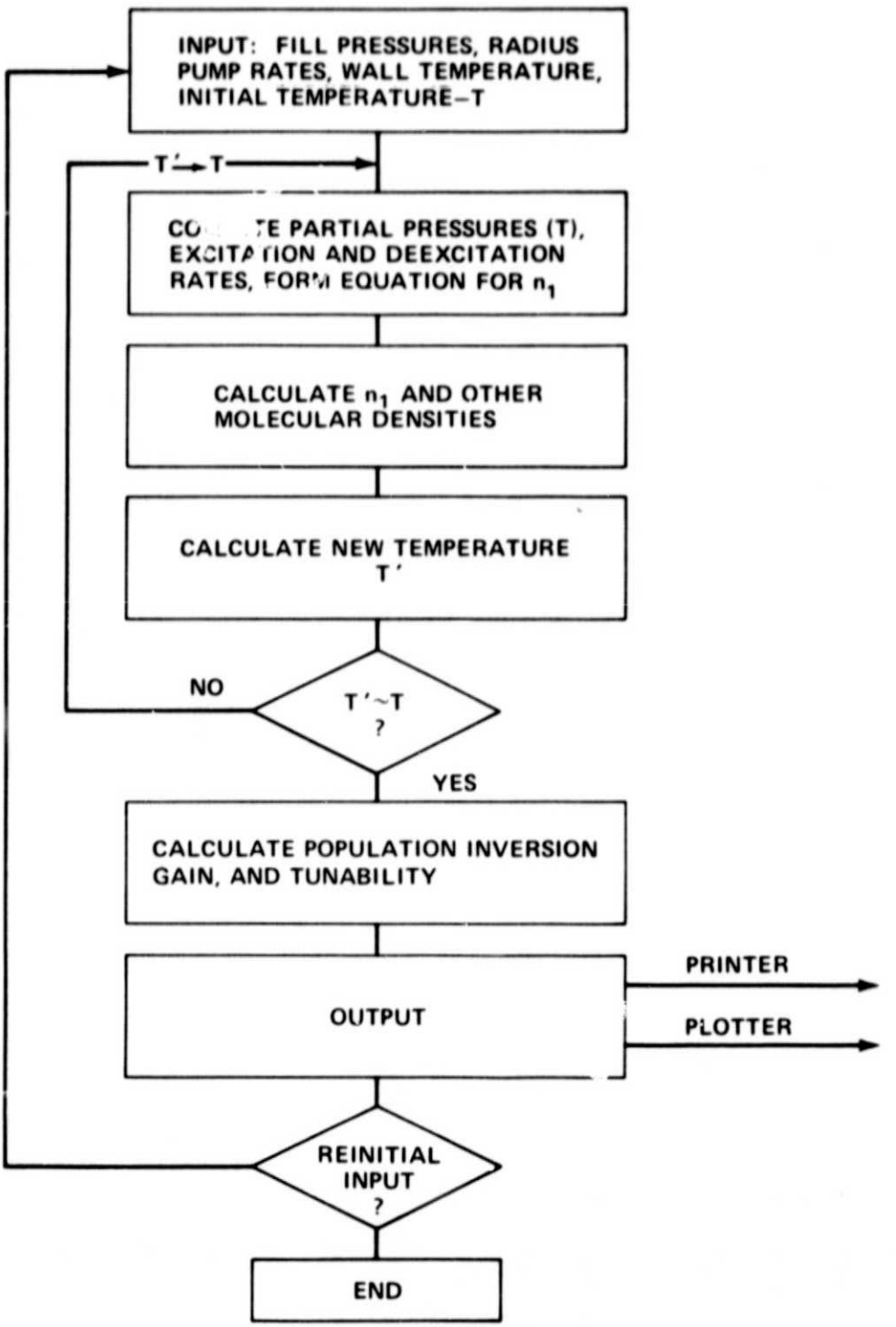

Figure 2. Logic flow diagram for computation of laser kinetic and discharge properties

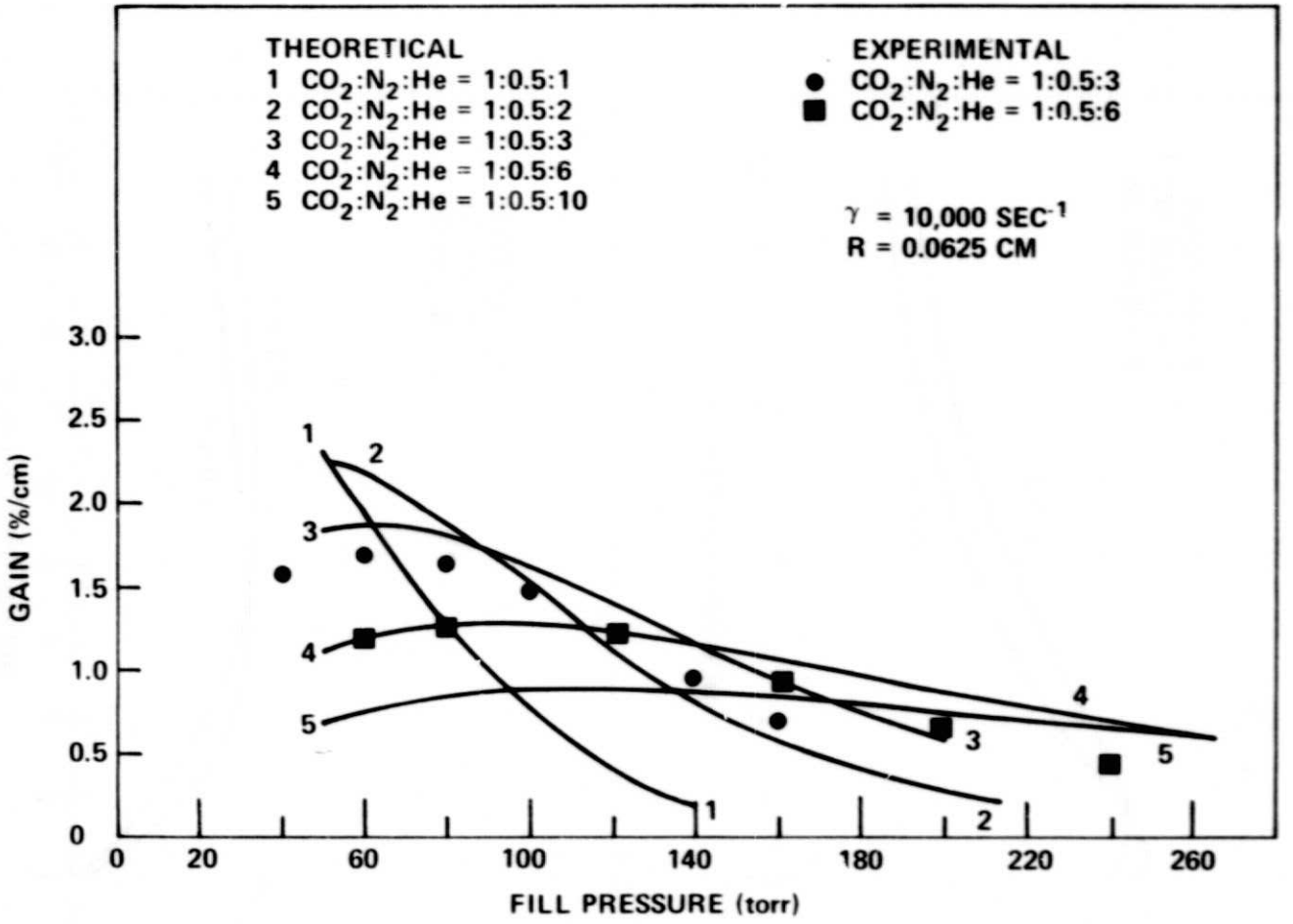

Figure 3. Small signal gain versus fill pressure for several gas mixtures. Gain is evaluated at line center assuming homogeneous line broadening. The experimental points are extracted from reference 12. We assume that $\gamma = 10,000\ sec^{-1}$ corresponds to a current of 2-3 ma for a 0.0625 cm bore radius.

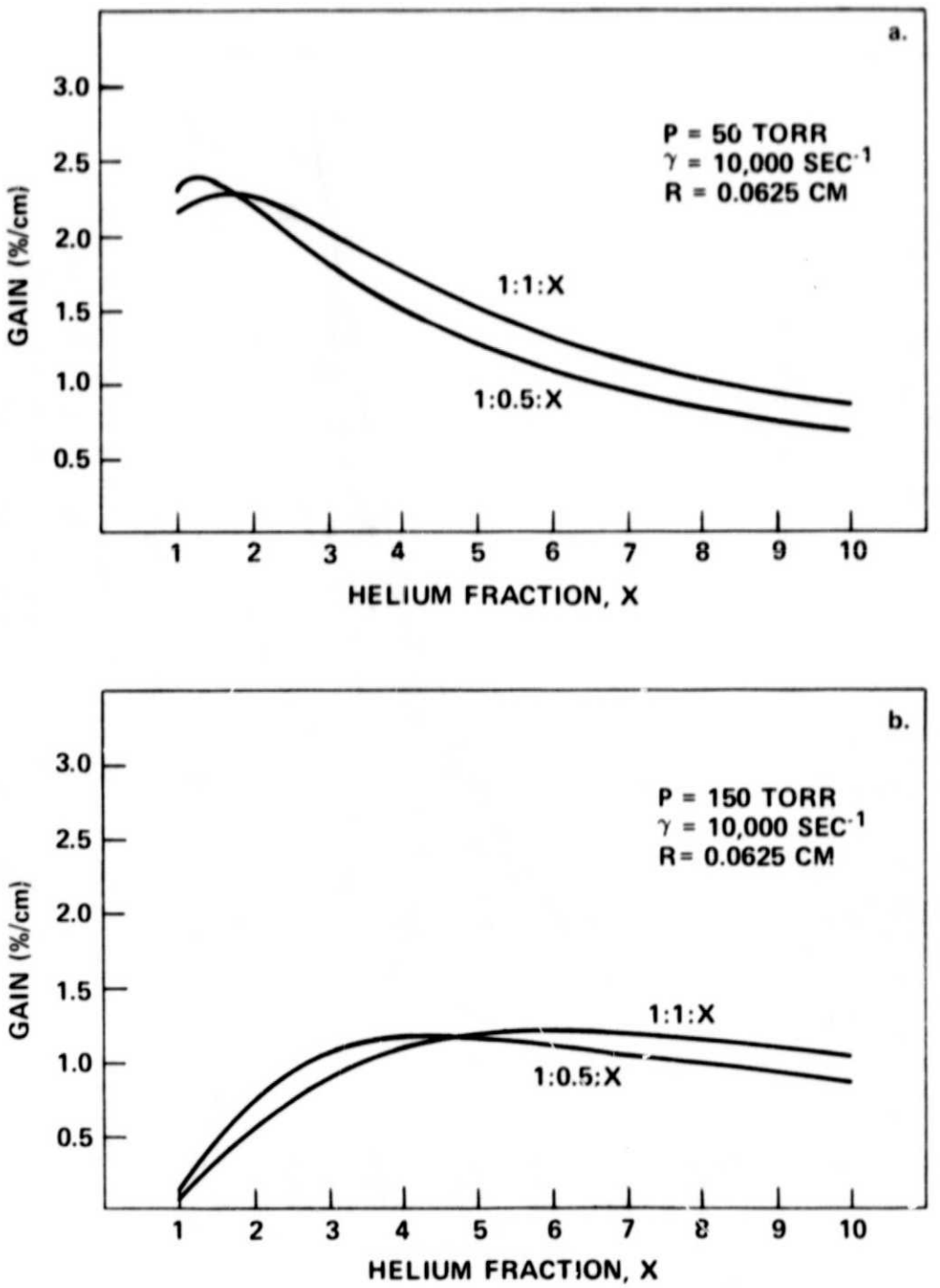

Figure 4. Small signal gain versus mixture for total fill pressure of (a) 50 torr (b) 150 torr

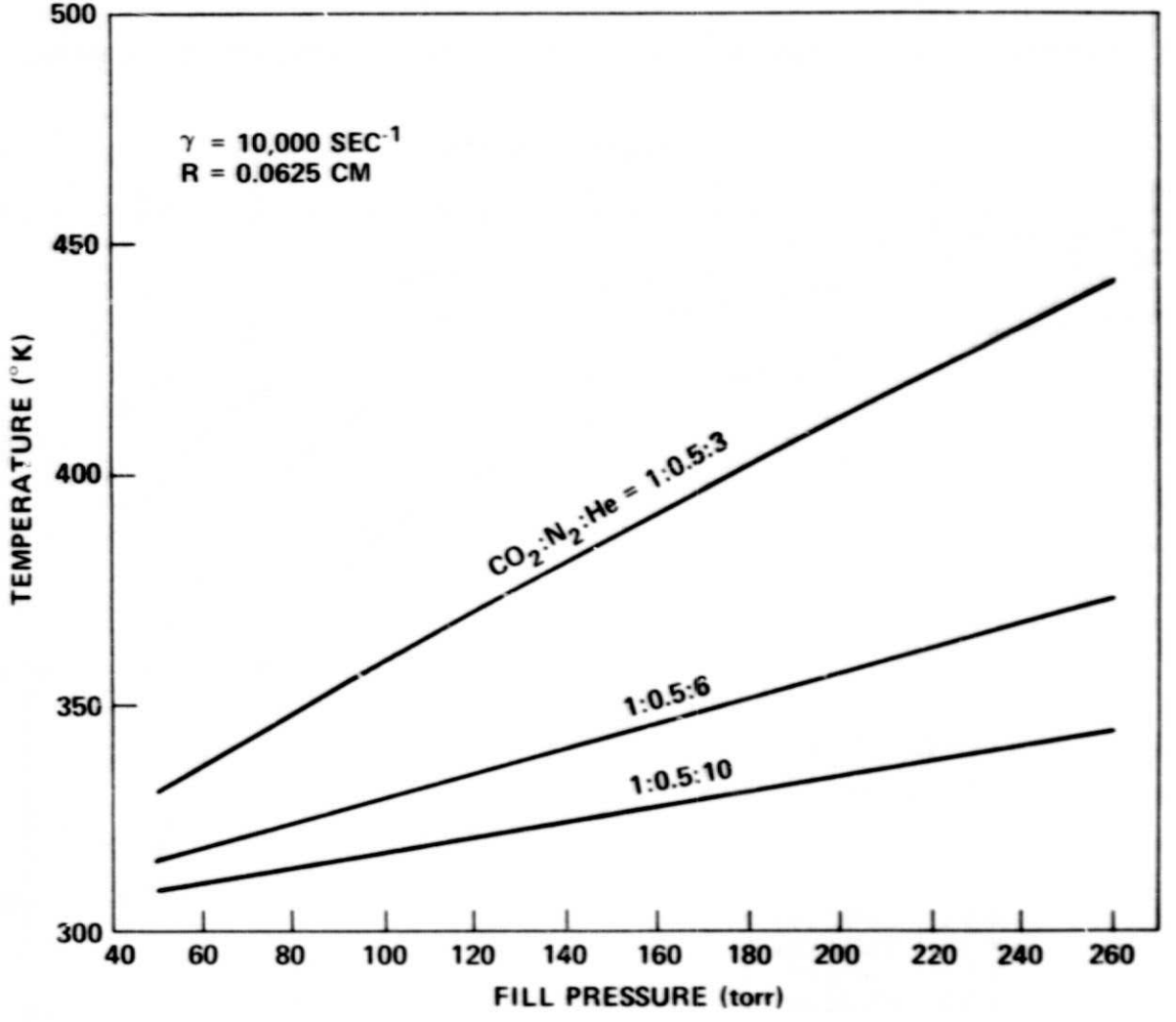

Figure 5. Temperature versus fill pressure for several gas mixtures

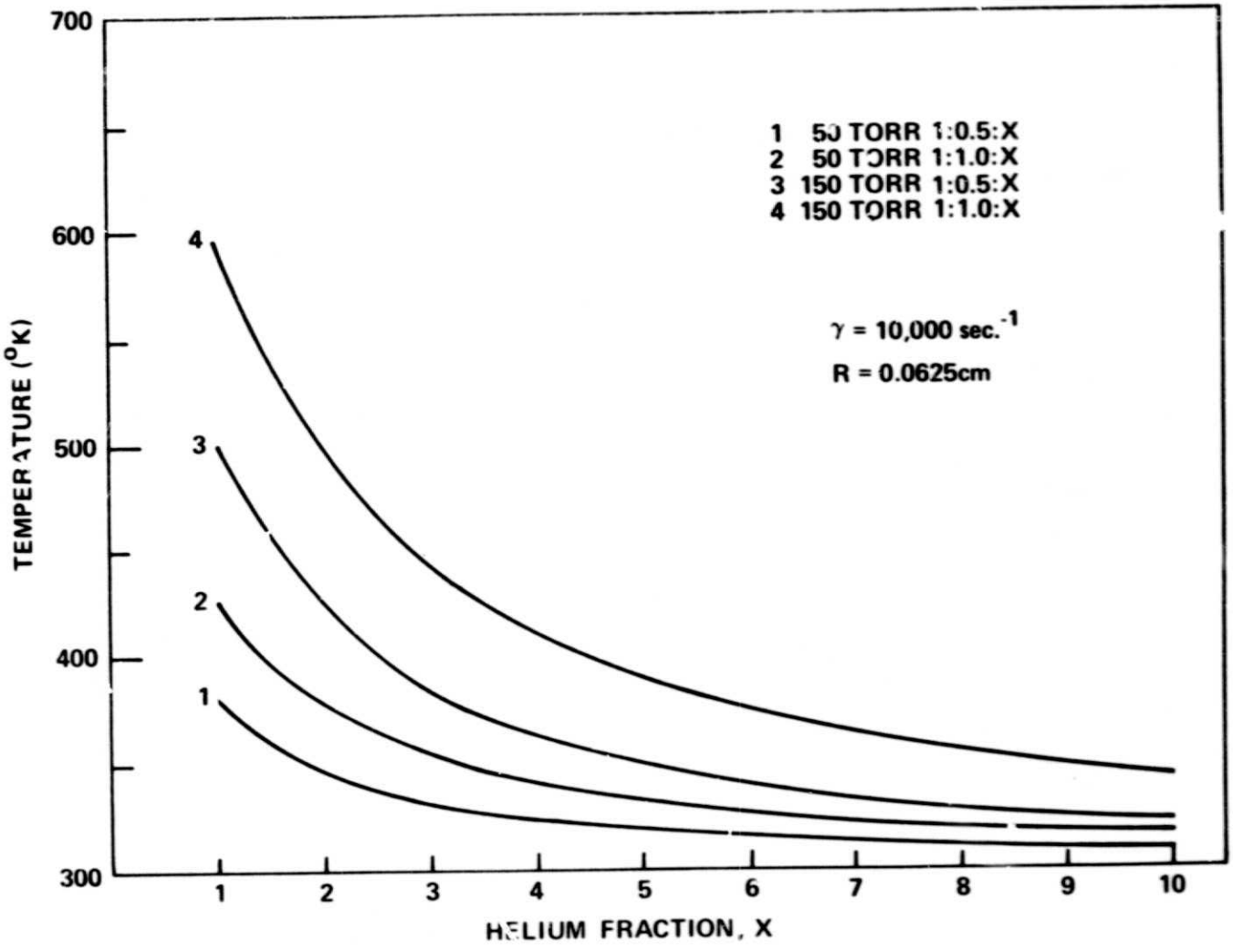

Figure 6. Temperature versus gas mixture of fill pressures of 50 and 150 torr

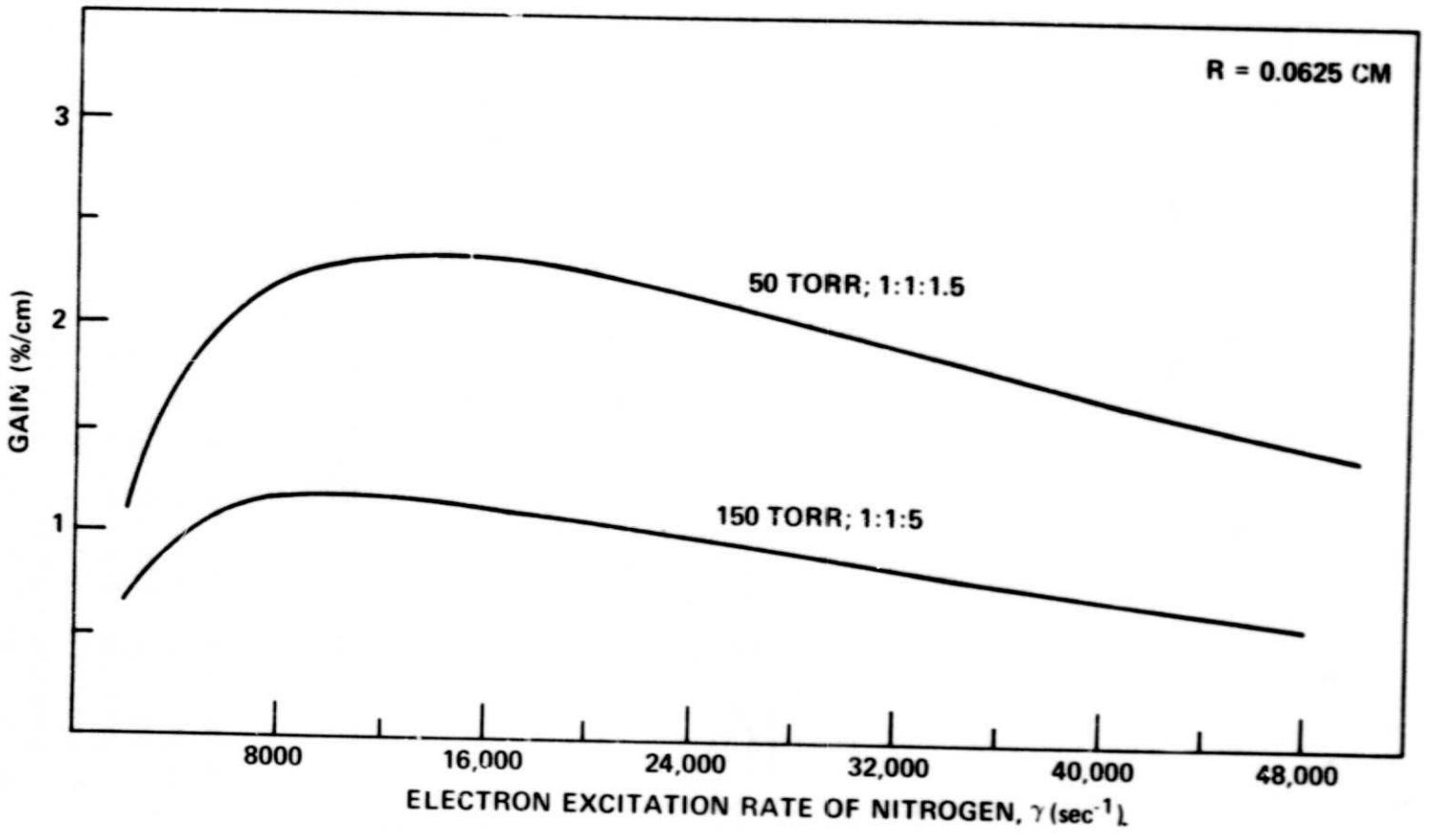

Figure 7. Small signal gain versus pump rate

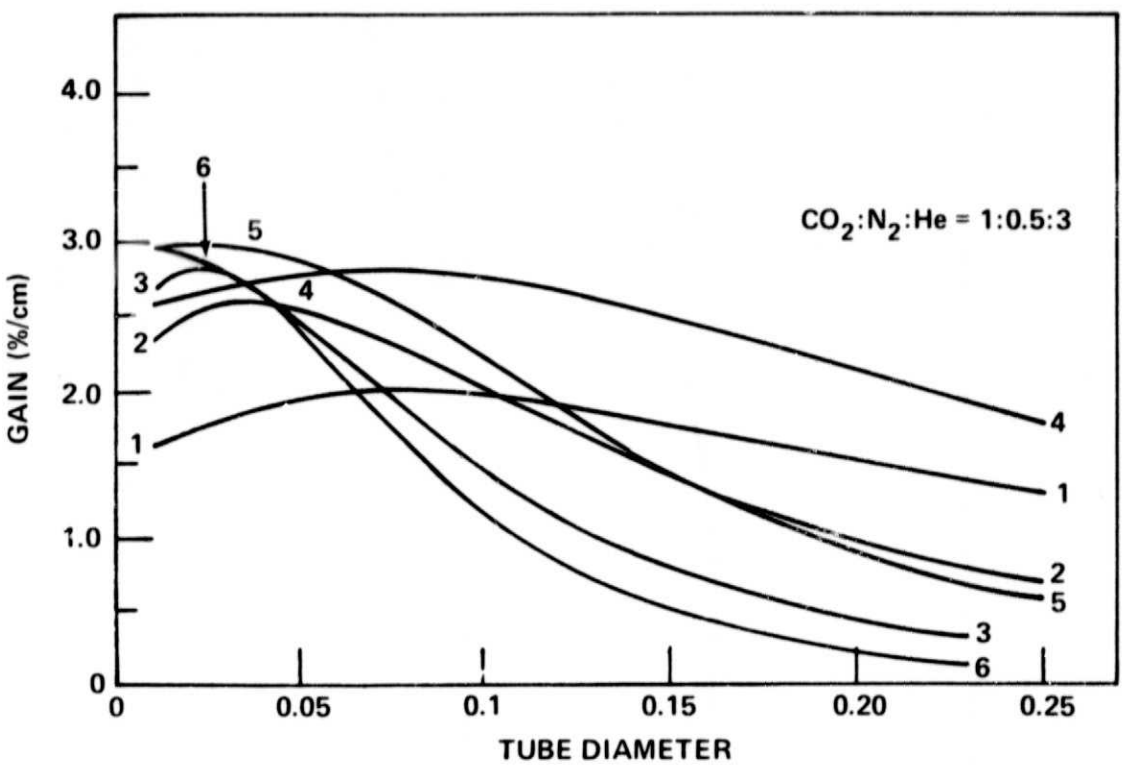

Figure 8. Small signal gain versus tube bore diameter.
1. pressure = 50 torr, $\gamma R^2 = 39$
2. pressure = 100 torr, $\gamma R^2 = 39$
3. pressure = 150 torr, $\gamma R^2 = 39$
4. pressure = 50 torr, $\gamma R^2 = 117$
5. pressure = 100 torr, $\gamma R^2 = 117$
6. pressure = 150 torr, $\gamma R^2 = 117$

$\gamma R^2 = 39$ (117) corresponds approximately to a current of 2 (6) ma.

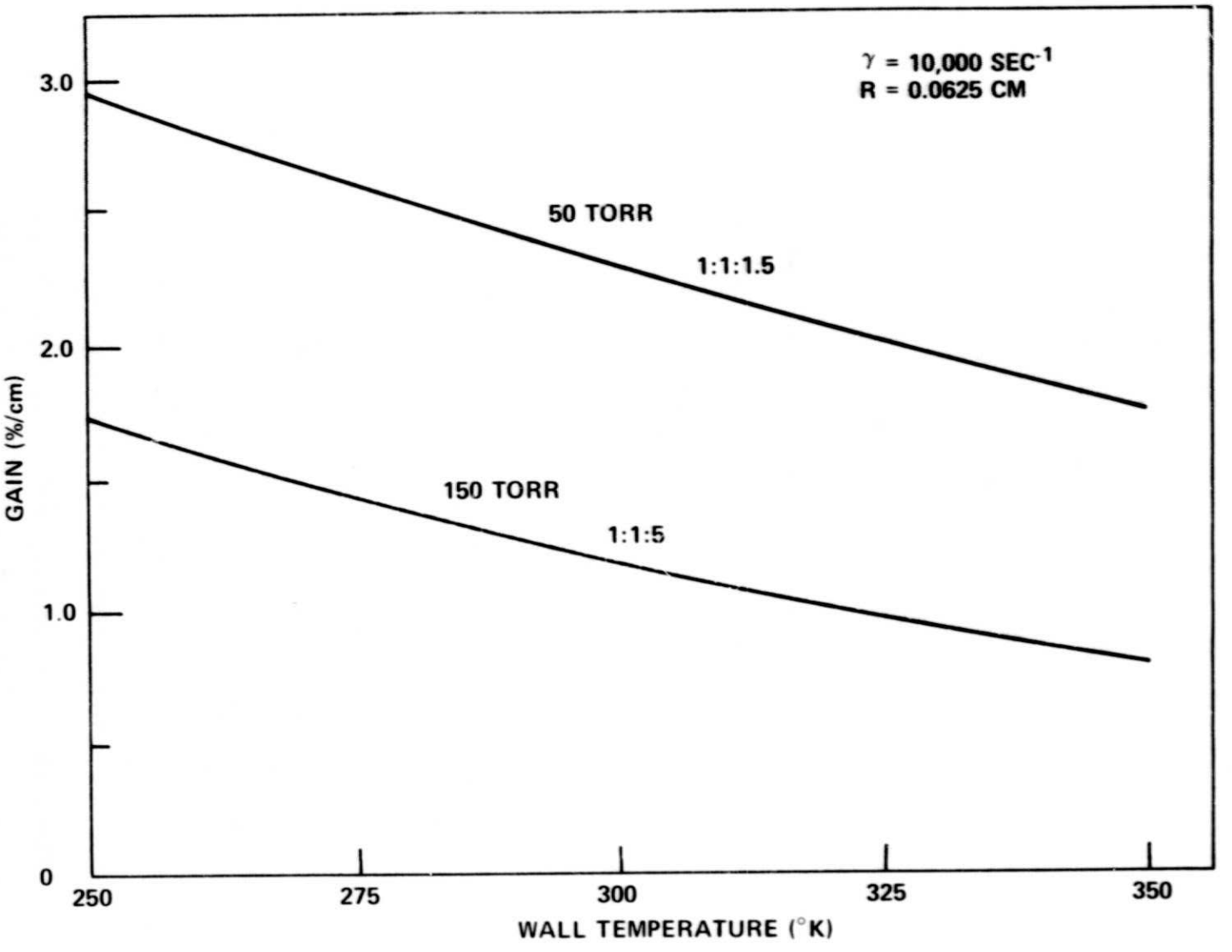

Figure 9. Small signal gain versus wall temperature

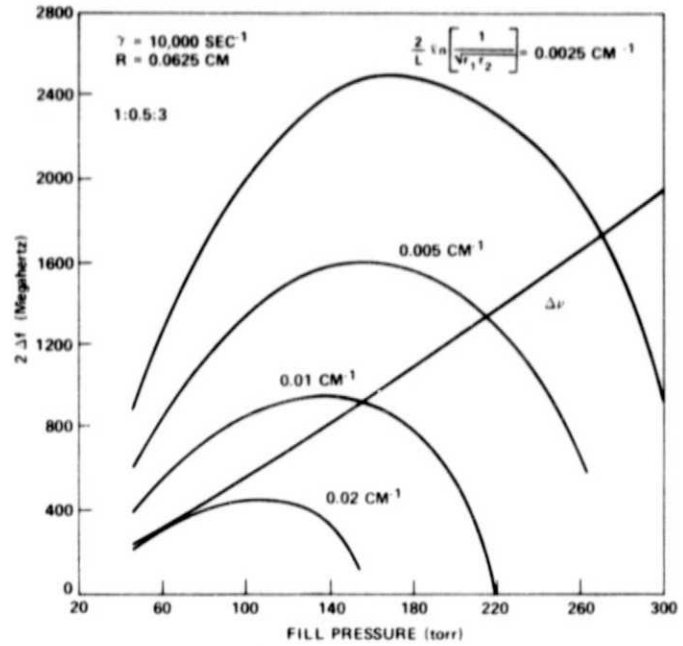

(a) gas mixture CO_2:N_2:He - 1:0.5:3

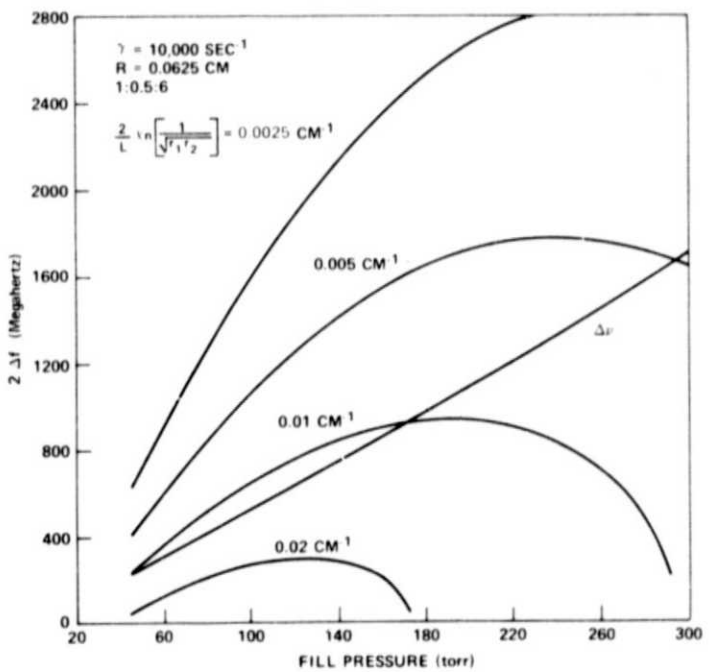

(b) gas mixture CO_2:N_2:He - 1:0.5:6

Figure 10. Laser tunability, $2\Delta f$, versus fill pressure. The parameter $\frac{2}{L} \ell n \sqrt{\frac{1}{r_1 r_2}}$ is essentially the loss divided by cavity length

Table Captions

Table I

Definitions of Symbols Appearing in Equation 3

Table II

References for Rate Constants Used to Obtain Numerical Results

Table I

Definitions of Symbols Appearing in Equation 3

Symbol	Definition
a	rate of electron excitation of ν_3 mode of CO_2 (sec^{-1})*
ζ	rate of electron deexcitation of ν_3 mode of CO_2 (sec^{-1})*
K	rate constant for vibrational energy exchange between excited states of N_2 and ν_3 mode of CO_2 (cm^{-3} sec^{-1})
K_{21}	rate of collisional transfer of energy from ν_3 to ν_{12} mode of CO_2 (sec^{-1})
K_{12}	rate for inverse process of K_{21} (sec^{-1})
K_{10}	rate of collisional deexcitation from ν_{12} mode to ground state (sec^{-1})
K_{01}	rate for inverse process of K_{10} (sec^{-1})
γ	rate of electron excitation of N_2 vibration (sec^{-1})*
ξ	rate of electron deexcitation of N_2 vibration (sec^{-1})*
D_{CO_2}	diffusion coefficient for CO_2 molecules (cm^2/sec)
D_{N_2}	diffusion coefficient for N_2 molecule (cm^2/sec)
Λ	(= R/2.4 where R is the tube radius) diffusion distance factor (cm)
n	density of CO_2 molecules (cm^{-3})
n_0	density of CO_2 molecules in ground state (cm^{-3})
n_1	density of CO_2 molecules with ν_{12} mode excited (cm^{-3})*
n_2	density of CO_2 molecules with ν_3 mode excited (cm^{-3})*
N_2	density of nitrogen molecules (cm^{-3})
N_2^0	density of nitrogen molecules in ground state (cm^{-3})
N_2^*	density of excited nitrogen molecules (cm^{-3})*
$\beta_1, \beta_2, \beta_{N_2}, \omega$	numerical coefficients

*These symbols refer to peak (on-axis value) in Equation 5 and thereafter.

Table II

References for Rate Constants Used to Obtain Numerical Results

Quantity	Reference
$K_{21}^{CO_2}, K_{21}^{N_2}, K_{21}^{He}$	1
$K_{10}^{CO_2}, K_{10}^{N_2}, K_{10}^{He}$	1
K	6
D_{CO_2}, D_{N_2}	1
$\kappa_{CO_2}, \kappa_{N_2}, \kappa_{He}$	7
$\Delta\nu$	8
B_1, B_2	9
t_2, t_S	10,2
$a \simeq \gamma/5$	